where $\theta_i \in \mathbb{S}^1$ and $\dot{\theta}_i \in \mathbb{R}^1$ are the generator rotor angle and frequency, $P_{\mathrm{m},i} > 0$ is the mechanical power input, and $M_i > 0$, and $D_i > 0$ are the inertia and damping coefficients.

We assume that each DC source is connected to the AC grid via an DC/AC inverter, the inverter output impendances are absorbed into the admittance matrix, and each inverter is equipped with a conventional droop-controller. For a droop-controlled inverter $i \in \mathcal{V}_3$ with droop-slope $1/D_i > 0$, the deviation of the power output $\sum_{j=1}^n a_{ij} \sin(\theta_i - \theta_j)$ from its nominal value $P_{\mathrm{d},i} > 0$ is proportional to the frequency deviation $D_i \dot{\theta}_i$. This gives rise to the inverter dynamics

$$D_i \dot{\theta}_i = P_{\mathrm{d},i} - \sum\nolimits_{j=1}^{n} a_{ij} \sin(\theta_i - \theta_j)\,, \quad i \in \mathcal{V}_3\,. \tag{6}$$

These power network devices are illustrated in Figure 3. Finally, we remark that different load models such as con-

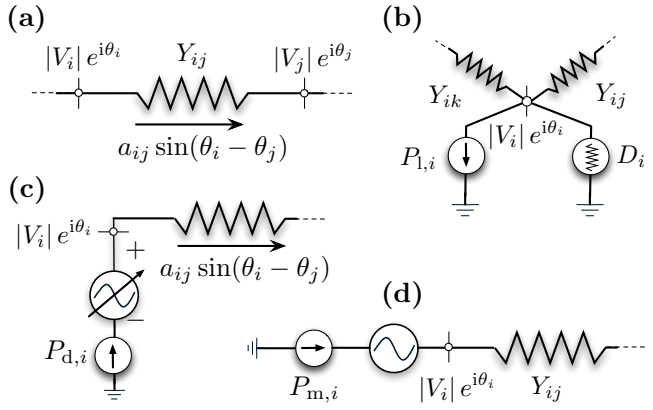

Fig. 3. Illustration of the power network devices as circuit elements. Subfigure (a) shows a transmission element connecting nodes i and j, Subfigure (b) shows a frequency-dependent load, Subfigure (c) shows an inverter controlled according to (6), and Subfigure (d) shows a synchronous generator.

stant power/current/susceptance loads and synchronous motor loads can be modeled and analyzed by the same set of equations (4)-(6), see [62]–[64], [116], [117].

Synchronization is pervasive in the operation of power networks. All generating units of an interconnected grid must remain in strict frequency synchronism while continuously following demand and rejecting disturbances. Notice that, with exception of the inertial terms $M_i \ddot{\theta}_i$ and the possibly non-unit coefficients D_i, the power network dynamics (4)-(6) are a perfect electrical analog of the coupled oscillator model (1) with $\omega = (-P_{\mathrm{l},i}, P_{\mathrm{m},i}, P_{\mathrm{d},i})$. Thus, it is not surprising that scientists from different disciplines recently advocated coupled oscillator approaches to analyze synchronization in power networks [43], [64], [69], [97], [114], [118]–[122].

The theoretic tools presented in the following sections establish how *frequency synchronization* in power networks depend on the nodal parameters $(P_{\mathrm{l},i}, P_{\mathrm{m},i}, P_{\mathrm{d},i})$ as well as the interconnecting electrical network with weights a_{ij}. Ultimately, this deep understanding of synchrony gives us the correct intuition to design controllers and remedial action schemes preventing the loss of synchrony.

C. Clock Synchronization in Decentralized Networks

Another emerging technological application of the coupled oscillator model (1) is clock synchronization in decentralized computing networks, such as wireless and distributed software networks. A natural approach to clock synchronization is to treat each clock as a coupled oscillator and follow a diffusion-based protocol to synchronize them, see the historic and recent surveys [36], [37], the landmark paper [38], and the interesting recent results [39]–[41].

Consider a set of distributed processors $\mathcal{V} = \{1, \ldots, n\}$ interconnected in a (possibly directed) communication network. Each processor is equipped with an internal software clock, and these clocks need to be synchronized for distributed computing and network routing tasks. For simplicity, we consider only analog clocks with continuous coupling since digital clocks are essentially discretized analog clocks and pulse-coupled clocks can be modeled continuously after a phase reduction and averaging analysis.

For our purposes, the clock of processor i is a voltage-controlled oscillator which outputs a harmonic waveform $s_i(t) = \sin(\theta_i(t))$, where $\theta_i(t)$ is the accumulated instantaneous phase. For uncoupled nodes, the phase $\theta_i(t)$ evolves as

$$\theta_i(t) = \left(\theta_i(0) + \frac{2\pi}{T_{\mathrm{nom}} + T_i} t\right) \mathrm{mod}(2\pi)\,, \quad i \in \{1, \ldots, n\}\,.$$

where $T_{\mathrm{nom}} > 0$ is the nominal period, $T_i \in \mathbb{R}$ is an offset (frequency offset or skew), and $\theta_i(0) \in \mathbb{S}^1$ is the initial phase. To synchronize their internal clocks, the processors follow a diffusion-based protocol. In a first step, neighboring oscillators continuously communicate their respective waveforms $s_i(t)$ to another. Second, through a phase detector each node measures a convex combination of phase differences as

$$\mathrm{cvx}_i(\theta(t)) = \sum\nolimits_{j=1}^{n} a_{ij} f(\theta_i(t) - \theta_j(t))\,, \quad i \in \{1, \ldots, n\}\,,$$

where $a_{ij} \geq 0$ are convex ($\sum_{j=1}^n a_{ij} = 1$) and detector-specific weights, and $f : \mathbb{S}^1 \to \mathbb{R}$ is an odd 2π-periodic function. Finally, $\mathrm{cvx}_i(\theta(t))$ is fed to a (first-order and constant) phase-locked loop filter K whose output drives the local phase according to

$$\dot{\theta}_i(t) = \frac{2\pi}{T_i} + K \cdot \mathrm{cvx}_i(\theta(t))\,, \quad i \in \{1, \ldots, n\}\,. \tag{7}$$

The goal of the synchronization protocol (7) is to synchronize the frequencies $\dot{\theta}_i(t)$ or even the phases $\theta_i(t)$ in the processor network. For an undirected communication protocol, symmetric weights $a_{ij} = a_{ji}$, and a sinusoidal coupling function $f(\cdot) = \sin(\cdot)$, the synchronization protocol (7) equals again the coupled oscillator model (1).

The tools developed in the next section will enable us to state conditions when the protocol (7) successfully achieves phase or frequency synchronization. Of course, the protocol (7) is merely a starting point, more sophisticated phase-locked loop filters can be constructed to enhance steady-state deviations from synchrony, and communication and phase noise as well as time-delays can be considered in the design.

D. Canonical Coupled Oscillator Model

The importance of the coupled oscillator model (1) does not stem only from the various examples listed in Sections I and II. Even though model (1) appears to be quite specific (a phase oscillator with constant driving term and continuous, diffusive, and sinusoidal coupling), it is the *canonical model* of coupled limit-cycle oscillators [123]. In the following, we briefly sketch how such general models can be reduced to model (1). We schematically follow the approaches [124, Chapter 10], [125] developed in the computational neuroscience community without aiming at mathematical precision, and we refer to [123], [126] for further details.

Consider an oscillator modeled as a dynamical system with state $x \in \mathbb{R}^m$ and nonlinear dynamics $\dot{x} = f(x)$, which admit a locally exponentially stable periodic orbit $\gamma \subset \mathbb{R}^m$ with period $T > 0$. By a change of variables, any trajectory in a local neighborhood of γ can be characterized by a phase variable $\varphi \in \mathbb{S}^1$ with dynamics $\dot{\varphi} = \Omega$, where $\Omega = 2\pi/T$.

Now consider a weakly forced oscillator of the form

$$\dot{x} = f(x) + \epsilon \cdot \delta(t)\,, \tag{8}$$

where $\epsilon > 0$ is sufficiently small and $\delta(t)$ is a time-dependent forcing term. For small forcing $\epsilon\delta(t)$, the attractive limit cycle γ persists, and the phase dynamics are obtained as

$$\dot{\varphi} = \Omega + \epsilon Q(\varphi)\delta(t) + \mathcal{O}(\epsilon^2)\,,$$

where $Q(\varphi)$ is the infinitesimal phase response curve (or linear response function), and we dropped higher order terms.

Now consider n such limit cycle oscillators, where $x_i \in \mathbb{R}^m$ is the state of oscillator i with limit cycle $\gamma_i \subset \mathbb{R}^m$ and period $T_i > 0$. We assume that the oscillators are weakly coupled with interaction graph $G(\mathcal{V}, \mathcal{E})$ and dynamics

$$\dot{x}_i = f_i(x_i) + \epsilon \sum\nolimits_{\{i,j\}\in\mathcal{E}} g_{ij}(x_i, x_j)\,,\ \ i \in \{1, \dots, n\}\,, \tag{9}$$

where $g_{ij}(\cdot)$ is the coupling function for the pair $\{i, j\} \in \mathcal{E}$. The coupling $g_{ij}(\cdot)$ can possibly be impulsive. The weak coupling in (9) can be identified with the weak forcing in (8), and a transformation to phase coordinates yields

$$\dot{\varphi}_i = \Omega_i + \epsilon \sum\nolimits_{\{i,j\}\in\mathcal{E}} Q_i(\varphi) g_{ij}(x_i(\varphi_i), x_j(\varphi_j))\,,$$

where $\Omega_i = 2\pi/T_i$. The local change of variables $\theta_i(t) = \varphi_i(t) - \Omega_i t$ then yields the coupled phase dynamics

$$\dot{\theta}_i = \epsilon \sum\nolimits_{\{i,j\}\in\mathcal{E}} Q_i(\theta_i + \Omega_i t) g_{ij}(x_i(\theta_i + \Omega_i t), x_j(\theta_j + \Omega_j t))\,.$$

An averaging analysis applied to the θ-dynamics results in

$$\dot{\theta}_i = \epsilon\omega_i + \epsilon \sum\nolimits_{\{i,j\}\in\mathcal{E}} h_{ij}(\theta_i - \theta_j)\,, \tag{10}$$

where $\omega_i = h_{ii}(0)$ and the averaged coupling functions are

$$h_{ij}(\chi) = \lim_{T\to\infty} \frac{1}{T} \int_0^T Q_i(\Omega_i\tau) g_{ij}(x_i(\Omega_i\tau), x_j(\Omega_j\tau - \chi)) d\tau.$$

Notice that the averaged coupling functions h_{ij} are 2π-periodic and the coupling is diffusive. If all functions h_{ij} are odd, a first-order Fourier series expansion of h_{ij} yields $h_{ij}(\cdot) \approx a_{ij}\sin(\cdot)$ as first harmonic with some coefficient a_{ij}. In this case, the dynamics (10) in the slow time scale $\tau = \epsilon t$ reduce exactly to the coupled oscillator model (1).

This analysis justifies calling the coupled oscillator model (1) the *canonical model* for coupled limit-cycle oscillators.

III. Synchronization Notions and Metrics

In this section, we introduce different notions of synchronization. Whereas the first four subsections address the commonly studied notions of synchronization associated with a coherent behavior and cohesive phases, Subsection III-E addresses the converse concept of phase balancing.

A. Synchronization Notions

The coupled oscillator model (1) evolves on $\mathbb{T}^n$, and features an important symmetry, namely the rotational invariance of the angular variable θ. This symmetry gives rise to the rich synchronization dynamics. Different levels of synchronization can be distinguished, and the most commonly studied notions are phase and frequency synchronization.

Phase synchronization: A solution $\theta : \mathbb{R}_{\geq 0} \to \mathbb{T}^n$ to the coupled oscillator model (1) achieves *phase synchronization* if all phases $\theta_i(t)$ become identical as $t \to \infty$.

Phase cohesiveness: As we will see later, phase synchronization can occur only if all natural frequencies ω_i are identical. If the natural frequencies are not identical, then each pairwise distance $|\theta_i(t) - \theta_j(t)|$ can converge to a constant but not necessarily zero value. The concept of phase cohesiveness formalizes this possibility. For $\gamma \in [0, \pi[$, let $\bar{\Delta}_G(\gamma) \subset \mathbb{T}^n$ be the closed set of angle arrays $(\theta_1, \dots, \theta_n)$ with the property $|\theta_i - \theta_j| \leq \gamma$ for all $\{i, j\} \in \mathcal{E}$, that is, each pairwise phase distance is bounded by γ. Also, let $\Delta_G(\gamma)$ be the interior of $\bar{\Delta}_G(\gamma)$. Notice that $\overline{\mathrm{Arc}}_n(\gamma) \subseteq \bar{\Delta}_G(\gamma)$ but the two sets are generally not equal. A solution $\theta : \mathbb{R}_{\geq 0} \to \mathbb{T}^n$ is then said to be *phase cohesive* if there exists a length $\gamma \in [0, \pi[$ such that $\theta(t) \in \bar{\Delta}_G(\gamma)$ for all $t \geq 0$.

Frequency synchronization: A solution $\theta : \mathbb{R}_{\geq 0} \to \mathbb{T}^n$ achieves *frequency synchronization* if all frequencies $\dot{\theta}_i(t)$ converge to a common frequency $\omega_{\text{sync}} \in \mathbb{R}$ as $t \to \infty$. The explicit synchronization frequency $\omega_{\text{sync}} \in \mathbb{R}$ of the coupled oscillator model (1) can be obtained by summing over all equations in (1) as $\sum_{i=1}^n \dot{\theta}_i = \sum_{i=1}^n \omega_i$. In the frequency-synchronized case, this sum simplifies to $\sum_{i=1}^n \omega_{\text{sync}} = \sum_{i=1}^n \omega_i$. In conclusion, if a solution of the coupled oscillator model (1) achieves frequency synchronization, then it does so with synchronization frequency equal to $\omega_{\text{sync}} = \sum_{i=1}^n \omega_i/n$. By transforming to a rotating frame with frequency ω_{sync} and by replacing ω_i by $\omega_i - \omega_{\text{sync}}$, we obtain $\omega_{\text{sync}} = 0$ (or equivalently $\omega \in \mathbf{1}_n^\perp$). In what follows, without loss of generality, we will sometimes assume that $\omega \in \mathbf{1}_n^\perp$ so that $\omega_{\text{sync}} = 0$.

*Remark 1 (***Terminology***):* Alternative terminologies for phase synchronization include full, exact, or perfect synchronization. For a frequency-synchronized solution all phase distances $|\theta_i(t) - \theta_j(t)|$ are constant in a rotating coordinate frame with frequency ω_{sync}, and the terminology *phase locking* is sometimes used instead of frequency synchronization. Other commonly used terms include frequency locking, frequency entrainment, or also partial synchronization. □

Synchronization: The main object under study in most applications and theoretic analyses are phase cohesive and frequency-synchronized solutions, that is, all oscillators rotate with the same synchronization frequency, and all their pairwise phase distances are bounded. In the following, we restrict our attention to synchronized solutions with sufficiently small phase distances $|\theta_i - \theta_j| \leq \gamma < \pi/2$ for $\{i,j\} \in \mathcal{E}$. Of course, there may exist other possible solutions, but these are not necessarily stable (see our analysis in Section IV) or not relevant in most applications[1]. We say that a solution $\theta : \mathbb{R}_{\geq 0} \to \mathbb{T}^n$ to the coupled oscillator model (1) is *synchronized* if there exists $\theta_{\text{sync}} \in \bar{\Delta}_G(\gamma)$ for some $\gamma \in [0, \pi/2[$ and $\omega_{\text{sync}} \in \mathbb{R}$ (identically zero for $\omega \in \mathbf{1}_n^\perp$) such that $\theta(t) = \theta_{\text{sync}} + \omega_{\text{sync}} \mathbf{1}_n t \pmod{2\pi}$ for all $t \geq 0$.

Synchronization manifold: The geometric object under study in synchronization is the synchronization manifold. Given a point $r \in \mathbb{S}^1$ and an angle $s \in [0, 2\pi]$, let $\text{rot}_s(r) \in \mathbb{S}^1$ be the rotation of r counterclockwise by the angle s. For $(r_1, \dots, r_n) \in \mathbb{T}^n$, define the equivalence class

$$[(r_1, \dots, r_n)] = \{(\text{rot}_s(r_1), \dots, \text{rot}_s(r_n)) \in \mathbb{T}^n \,|\, s \in [0, 2\pi]\}.$$

Clearly, if $(r_1, \dots, r_n) \in \bar{\Delta}_G(\gamma)$ for some $\gamma \in [0, \pi/2[$, then $[(r_1, \dots, r_n)] \subset \bar{\Delta}_G(\gamma)$. Given a synchronized solution characterized by $\theta_{\text{sync}} \in \bar{\Delta}_G(\gamma)$ for some $\gamma \in [0, \pi/2[$, the set $[\theta_{\text{sync}}] \subset \bar{\Delta}_G(\gamma)$ is a *synchronization manifold* of the coupled-oscillator model (1). Note that a synchronized solution takes value in a synchronization manifold due to rotational symmetry, and for $\omega \in \mathbf{1}_n^\perp$ (implying $\omega_{\text{sync}} = 0$) a synchronization manifold is also an equilibrium manifold of the coupled oscillator model (1). These geometric concepts are illustrated in Figure 4 for the two-dimensional case.

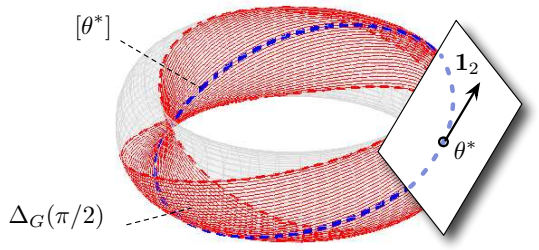

Fig. 4. Illustration of the state space $\mathbb{T}^2$, the set $\Delta_G(\pi/2)$, the synchronization manifold $[\theta^*]$ associated to a phase-synchronized angle array $\theta^* = (\theta_1^*, \theta_2^*) \in \bar{\Delta}_G(0)$, and the tangent space with translation vector $\mathbf{1}_2$ at θ^*.

B. A Simple yet Illustrative Example

The following example illustrates the different notions of synchronization introduced above and points out various important geometric subtleties occurring on the compact state space $\mathbb{T}^2$. Consider $n = 2$ oscillators with $\omega_2 \geq 0 \geq \omega_1 = -\omega_2$. We restrict our attention to angles contained in an open half-circle: for angles θ_1, θ_2 with $|\theta_2 - \theta_1| < \pi$, the *angular difference* $\theta_2 - \theta_1$ is the number in $]-\pi, \pi[$ with magnitude equal to the geodesic distance $|\theta_2 - \theta_1|$ and with positive sign if and only if the counter-clockwise path length from θ_1 to θ_2 on $\mathbb{T}^1$ is smaller than the clockwise path length. With this definition the two-dimensional oscillator dynamics $(\dot\theta_1, \dot\theta_2)$ can be reduced to the scalar difference dynamics $\dot\theta_2 - \dot\theta_1$. After scaling time as $t \mapsto t(\omega_2 - \omega_1)$ and introducing $\kappa = 2a_{12}/(\omega_2 - \omega_1)$ the difference dynamics are

$$\frac{d}{dt}(\theta_2 - \theta_1) = f_\kappa(\theta_2 - \theta_1) := 1 - \kappa \sin(\theta_2 - \theta_1). \quad (11)$$

The scalar dynamics (11) can be analyzed graphically by plotting the vector field $f_\kappa(\theta_2 - \theta_1)$ over the difference variable $\theta_2 - \theta_1$, as in Figure 5(a). Figure 5(a) displays a saddle-node bifurcation at $\kappa = 1$. For $\kappa < 1$ no equilibrium of (11) exists, and for $\kappa > 1$ an asymptotically stable equilibrium $\theta_{\text{stable}} = \arcsin(\kappa^{-1}) \in]0, \pi/2[$ together with a saddle point $\theta_{\text{saddle}} = \arcsin(\kappa^{-1}) \in]\pi/2, \pi[$ exists.

For $\theta(0) \in \text{Arc}_n(|\theta_{\text{saddle}}|)$ all trajectories converge exponentially to θ_{stable}, that is, the oscillators synchronize exponentially. Additionally, the oscillators are phase cohesive if an only if $\theta(0) \in \overline{\text{Arc}}_n(|\theta_{\text{saddle}}|)$, where all trajectories remain bounded. For $\theta(0) \notin \overline{\text{Arc}}_n(|\theta_{\text{saddle}}|)$ the difference $\theta_2(t) - \theta_1(t)$ will increase beyond π, and by definition will change its sign since the oscillators change orientation. Ultimately, $\theta_2(t) - \theta_1(t)$ converges to the equilibrium θ_{stable} in the branch where $\theta_2 - \theta_1 < 0$. In the configuration space $\mathbb{T}^2$ this implies that the distance $|\theta_2(t) - \theta_1(t)|$ increases to its maximum value π and shrinks again, that is, the oscillators are not phase cohesive and revolve once around the circle before converging to the equilibrium manifold. Since $\sin(\theta_{\text{stable}}) = \sin(\theta_{\text{saddle}}) = \kappa^{-1}$, strongly coupled oscillators with $\kappa \gg 1$ practically achieve phase synchronization from every initial condition in an open semi-circle. In the critical case, $\kappa = 1$, the saddle equilibrium manifold at $\pi/2$ is globally attractive but not stable. An representative trajectory is illustrated in Figure 5(b).

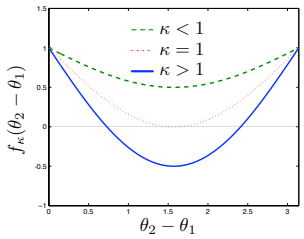

(a) Vector field (11) for $\theta_2 - \theta_1 > 0$

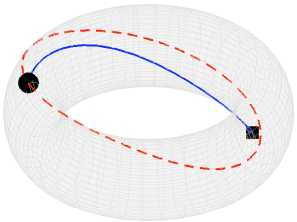

(b) Trajectory $\theta(t)$ for $\kappa = 1$

Fig. 5. Plot of the vector field (11) for various values of κ and a trajectory $\theta(t) \in \mathbb{T}^2$ for the critical case $\kappa = 1$, where the dashed line is the saddle equilibrium manifold and ■ and ● depict $\theta(0)$ and $\lim_{t\to\infty} \theta(t)$. The non-smoothness of the vector field $f(\theta_2 - \theta_1)$ at the boundaries $\{0, \pi\}$ is an artifact of the non-smoothness of the geodesic distance on $\mathbb{T}^2$

In conclusion, the simple but already rich 2-dimensional case shows that two oscillators are phase cohesive and synchronize if and only if $\kappa > 1$, that is, if and only if the coupling dominates the non-uniformity as $2a_{12} > \omega_2 - \omega_1$. The ratio $1/\kappa$ determines the ultimate phase cohesiveness as

[1]For example, in power network applications the coupling terms $a_{ij} \sin(\theta_i - \theta_j)$ are power flows along transmission lines $\{i,j\} \in \mathcal{E}$, and the phase distances $|\theta_i - \theta_j|$ are bounded well below $\pi/2$ due to thermal constraints. In Subsection III-E, we present a converse synchronization notion, where the goal is to maximize phase distances.